

MULTIPHASE MEAN CURVATURE FLOWS APPROXIMATION: THE CASE OF NON HARMONICALLY ADDITIVE MOBILITIES

ERIC BONNETIER, ELIE BRETIN, AND SIMON MASNOU

ABSTRACT. This paper concerns the robust approximation of multi-phase mean curvature flow by phase fields even when the phase mobility are highly contrasted. Recent work suggested that harmonically additive mobilities could be incorporated in the metric of the associated gradient flow. We generalize this approach to arbitrary mobilities, by splitting them as a sum of a harmonically additive mobilities. We establish the consistency of the resulting method, by analyzing the sharp interface limit of the flow : a formal expansion of the phase field shows that the method is of order 2. Finally, we present some numerical experiments in dimensions 2 and 3 that illustrate the interest of our method, in particular in the modeling of flows in which some of the phases have 0 mobility.

1. INTRODUCTION

1.1. Evolution by mean curvature of single-phase flow.

Motion by mean curvature is the driving mechanism of many physical systems, in which interfaces are moving due to the thermodynamics of phase changes. Such situations are encountered in the modeling of epitaxial growth of thin films [10], in the fabrication of nano-wire by vapor-liquid-solid growth [12, 33], in the modeling of wetting or de-wetting of substrates by crystalline materials [7, 16], or in the evolution of grain boundaries in poly-crystalline materials [27].

A collection of sets $t \rightarrow \Omega(t) \subset \mathbb{R}^d$ evolves via motion by mean curvature if at each point $x \in \partial\Omega(t)$, the normal velocity $V(x)$ is proportional to the mean curvature $H(x)$. Up to a time rescaling, the equation of evolution takes the form

$$V(x) = H(x), \quad x \in \partial\Omega(t),$$

and can be viewed as the L^2 -gradient flow of the perimeter of the sets $\Omega(t)$

$$P(\Omega(t)) = \mathcal{H}^{d-1}(\partial\Omega(t)),$$

where \mathcal{H}^{d-1} denotes the $d - 1$ dimensional Hausdorff measure. The seminal work of Modica and Mortola [25] has shown that the perimeter ‘energy’ can be approximated by the smooth Van der Waals/Cahn-Hilliard functional

$$(1) \quad P_\varepsilon(u) = \int_Q \left(\frac{\varepsilon}{2} |\nabla u|^2 + \frac{1}{\varepsilon} W(u) \right) dx.$$

where $Q \subset \mathbb{R}^2$ is a large enough fixed bounded box, $\varepsilon > 0$ is a small parameter and W is a smooth double-well potential, typically

$$W(s) = \frac{1}{2} s^2 (1 - s)^2.$$

It is proved in [25], that when Ω is a set of finite perimeter, its characteristic function 1_Ω can be approximated in the sense of Γ -convergence for the L^1 topology, by sequences of functions of the form $u_\varepsilon = q(\text{dist}(x, \Omega)/\varepsilon)$, which satisfy $P_\varepsilon(u_\varepsilon) \rightarrow c_W P(\Omega)$, with $c_W = \int_0^1 \sqrt{2W(s)} ds$. Here, $\text{dist}(x, \Omega)$ denotes the signed distance to the set Ω .

2020 *Mathematics Subject Classification.* 74N20, 35A35, 53E10, 53E40, 65M32, 35A15.

Key words and phrases. Phase field approximation, Allen-Cahn system, mobilities, numerical approximation.

The *optimal profile* q , depends on the potential W , and is given by

$$q = \operatorname{argmin}_p \left\{ \int_{\mathbb{R}} \sqrt{W(p(s))} |p'(s)| ds, p(-\infty) = 1, p(0) = 1/2, p(+\infty) = 0 \right\},$$

where p ranges over the set of Lipschitz continuous functions $p : \mathbb{R} \rightarrow \mathbb{R}$. A simple derivation of the Euler equation associated with this minimization problem shows that

$$(2) \quad q'(s) = -\sqrt{2W(q(s))} \quad \text{and} \quad q''(s) = W'(q(s)), \quad \text{for all } s \in \mathbb{R},$$

which implies that $q(s) = (1 - \tanh(s))/2$ in the case of the standard double well potential $W(s) = \frac{1}{2}s^2(1 - s)^2$ considered above.

The L^2 -gradient flow of the Van der Waals–Cahn–Hilliard energy P_ε , results in the Allen–Cahn equation [1]. Up to a time rescaling, it takes the form

$$(3) \quad u_t = \Delta u - \frac{1}{\varepsilon^2} W'(u).$$

This nonlinear parabolic equation has a unique solution, which satisfies a comparison principle, see for instance [2, chap 14]. Further, a smooth set Ω evolving by mean curvature flow can be approximated by

$$\Omega^\varepsilon(t) = \left\{ x \in \mathbb{R}^d, u^\varepsilon(x, t) \geq \frac{1}{2} \right\},$$

where u^ε solves (3) with initial condition

$$u^\varepsilon(x, 0) = q \left(\frac{\operatorname{dist}(x, \Omega(0))}{\varepsilon} \right).$$

A formal asymptotic expansion of u^ε near the interfaces [4] shows that u^ε is quadratically close to the optimal profile, i.e.

$$u^\varepsilon(x, t) = q \left(\frac{\operatorname{dist}(x, \Omega^\varepsilon(t))}{\varepsilon} \right) + O(\varepsilon^2),$$

where the associated normal velocity V^ε satisfies

$$V^\varepsilon = H + O(\varepsilon^2).$$

Convergence of $\partial\Omega_\varepsilon(t)$ to $\partial\Omega(t)$ has been rigorously proved for smooth flows in [18, 26, 5] with a quasi-optimal convergence order $O(\varepsilon^2 |\log \varepsilon|^2)$. The fact that u^ε is quadratically close to the optimal profile has inspired the development of very effective numerical methods [25, 18, 8, 30, 11].

1.2. Multiphase flows.

In the presence of several phases, the motion of interfaces obeys a relation of the form

$$V_{ij} = m_{ij} \sigma_{ij} H_{ij},$$

where V_{ij} , H_{ij} and σ_{ij} denote the normal velocity, mean curvature and surface tension along an interface Γ_{ij} that separates the phases i and j . The mobilities m_{ij} describe how fast adatoms from one phase may be adsorbed in another phase as the front advances. These parameters are associated with the kinetics of the moving front, not with the equilibrium shape of the crystal, contrarily to the surface tensions σ_{ij} .

Assuming that the material phases partition a region $Q \subset \mathbb{R}^n$, $n = 2, 3$ into closed sets Ω_i occupied by the phase i , the perimeter functional takes the form

$$P(\Omega_1, \Omega_2, \dots, \Omega_N) = \frac{1}{2} \sum_{1 \leq i < j \leq N} \sigma_{ij} \mathcal{H}^{d-1}(\Gamma_{ij}).$$

We assume throughout this work that the surface tensions are additive, i.e., that there exist $\sigma_i \geq 0, 1 \leq i \leq N$, such that

$$\sigma_{ij} = \sigma_i + \sigma_j, \quad 1 \leq i < j \leq N.$$

This assumption is always satisfied when $N \leq 3$ and when the set of coefficients σ_{ij} satisfy the triangle inequality. In particular, this is the case of the evolution of a single chemical species in its liquid, vapor and solid phases. The perimeter functional can be rewritten in the form

$$P(\Omega_1, \Omega_2, \dots, \Omega_N) = \sum_i^N \sigma_i \mathcal{H}^{d-1}(\partial\Omega_i),$$

and therefore lends itself to approximation by the multiphase Cahn-Hilliard energy defined for $\mathbf{u} = (u_1, u_2, \dots, u_N)$ by

$$P_\varepsilon(\mathbf{u}) = \begin{cases} \frac{1}{2} \sum_{i=1}^N \int_Q \sigma_i \left(\varepsilon \frac{|\nabla u_i|^2}{2} + \frac{1}{\varepsilon} W(u_i) \right) dx, & \text{if } \sum_{i=1}^N u_i = 1, \\ +\infty & \text{otherwise.} \end{cases}$$

The Modica-Mortola Γ -convergence result of P_ε to $c_W P$ was generalized to the multi-phase case in [28] when $\sigma_i = 1, 1 \leq i \leq N$. For more general Γ -convergence results, we refer to [3, 14] for inhomogeneous surface tensions, and to [21, 20] for anisotropic surface tensions.

The L^2 -gradient flow of P_ε yields the following system of Allen-Cahn equations

$$(4) \quad \partial_t u_k^\varepsilon = \sigma_k \left[\Delta u_k^\varepsilon - \frac{1}{\varepsilon^2} W'(u_k^\varepsilon) \right] + \lambda^\varepsilon, \quad \forall k = 1, \dots, N,$$

where the Lagrange multiplier λ^ε accounts for the constraint $\sum_{k=1}^N u_k^\varepsilon = 1$. In practice however, the numerical schemes derived from (4) do not prove as accurate as in the single-phase case. To improve the convergence, one may localize the Lagrange multiplier λ near the diffuse interface, as was proposed in [13], and consider instead of (4) the modified system

$$(5) \quad \partial_t u_k^\varepsilon = \sigma_k \left[\Delta u_k^\varepsilon - \frac{1}{\varepsilon^2} W'(u_k^\varepsilon) \right] + \lambda^\varepsilon \sqrt{2W(u_k)} \quad \forall k = 1, \dots, N,$$

where the effect of λ is essentially felt in the vicinity of the interfaces. A rigorous proof of convergence of this modified Allen-Cahn system to multi-phase Brakke's mean curvature flow is established in [32].

1.3. Incorporating mobilities.

As mentioned above, mobilities are kinetic parameters that model how fast adatoms get attached to an evolving front. In [20, 21], mobilities are included in the definition of the surface potential $f(\mathbf{u}, \nabla \mathbf{u})$ and of the multi-well potential $\mathbf{W}(\mathbf{u})$, that define the Allen-Cahn approximate energy $\mathbf{u} = (u_1, u_2, \dots, u_N)$ by

$$P_\varepsilon(\mathbf{u}) = \begin{cases} \int_Q \varepsilon f(\mathbf{u}, \nabla \mathbf{u}) + \frac{1}{\varepsilon} \mathbf{W}(\mathbf{u}) dx, & \text{if } \sum_{i=1}^N u_i = 1, \\ +\infty & \text{otherwise.} \end{cases}$$

An example of surface potential f and multiple well potential \mathbf{W} that has been considered is

$$\begin{cases} f(\mathbf{u}, \nabla \mathbf{u}) &= \sum_{i < j} m_{ij} \sigma_{ij} |u_i \nabla u_j - u_j \nabla u_i|^2, \\ \mathbf{W}(\mathbf{u}) &= \sum_{i < j} \frac{\sigma_{ij}}{m_{ij}} u_i^2 u_j^2 + \sum_{i < j < k} \sigma_{ijk} u_i^2 u_j^2 u_k^2. \end{cases}$$

In these models, both surface tensions and mobilities appear in the Cahn-Hilliard energy. It is shown in [22, 21] that taking the sharp interface limit imposes constraints on the limiting values of the surface tensions and mobilities, in particular in the anisotropic case. From a numerical perspective it follows that the mobilities are likely to impact the size of the diffuse

interfaces, as they appear in the energy, especially in situations where the contrast of mobilities is large.

In this work, we assume that the flux of adatoms is a linear function of the normal velocity of the interface Γ_{ij} , with a proportionality constant equal to m_{ij} . From the modeling point of view, this amounts to considering the surface tensions are geometric parameters which govern the equilibrium, and the mobilities as parameters related to the evolution of the system from an out-of-equilibrium configuration, which only affect the metric used for the gradient flow.

It is suggested in [12] that mobilities could be taken into account through the metric with which the gradient flow is performed. In that work, mobilities are considered that mimic the properties of additive surface tensions, i.e., it is assumed that the m_{ij} 's can be decomposed as

$$(6) \quad \frac{1}{m_{ij}} = \frac{1}{m_i} + \frac{1}{m_j},$$

for some $m_j > 0, 1 \leq j \leq N$. The associated Allen Cahn system took then the form

$$(7) \quad \partial_t u_k^\varepsilon = m_k \left[\sigma_k \left(\Delta u_k^\varepsilon - \frac{1}{\varepsilon^2} W'(u_k^\varepsilon) \right) + \lambda^\varepsilon \sqrt{2W(u_k)} \right], \quad \forall k \in \{1, 2, \dots, N\},$$

where the Lagrange multiplier λ^ε is again associated to the constraint $\sum u_i^\varepsilon = 1$ and given by

$$\lambda^\varepsilon = - \frac{\sum_k m_k \sigma_k \left(\Delta u_k^\varepsilon - \frac{1}{\varepsilon^2} W'(u_k^\varepsilon) \right)}{\sum_k m_k \sqrt{2W(u_k)}}.$$

This model has the following advantages:

- It is quantitative in the sense that the coefficients σ_i and m_i can be identified from the mobilities and surface tensions m_{ij} and σ_{ij} ,
- Numerical tests indicate accuracy of order two in ε and that the size of the diffuse interface does not depend on the m_{ij} 's,
- A simple and efficient numerical scheme can be derived to approximate the solutions to (7).

We call mobilities that satisfy (6) harmonically additive mobilities. For convenience, we extend this definition to cases when some of the m_i 's vanish, and consider that the corresponding Allen Cahn equation is stationary, i.e., reduces to $\partial_t u_i^\varepsilon = 0$.

1.4. General mobilities.

The main motivation of the paper is to introduce a phase field model similar to (7), but not limited to harmonically additive mobilities. For example, in the case of a 3-phase system ($N = 3$), the triple of mobility coefficients $(m_{12}, m_{13}, m_{23}) = (1, 0, 0)$ is indeed harmonically additive as one can choose $m_1 = m_2 = 2$ and $m_3 = 0$. However, this is far from general, and there seems to be no physical (even practical) reason that justifies this hypothesis. The situation studied in [12], that models the vapor-liquid-solid (VLS) growth of nanowires, is an illustration of this remark. Indeed, VLS growth can be viewed as a system of 3 phases with mobilities $m_{LS} = m_{LV} = 1, m_{SV} = 0$. In such a system, the vapor-solid interface remains fixed, as growth only takes place along the liquid-solid interface. It is easy to check that a triple of mobilities of the form $(m_{12}, m_{13}, m_{23}) = (1, 1, 0)$ fails to be additive (or more generally, any triple $(1, 1, \beta)$ as soon as $\beta < 1/2$).

To derive a numerical scheme for which the width of the diffuse interface does not depend on the possible degeneracy of the mobilities, we express the set mobilities as a sum of harmonically additive mobilities. In other words, we assume that there exists $P \in \mathbb{N}$ and positive coefficients m_{ij}^p and m_i^p such that

$$(8) \quad m_{ij} = \sum_{p=1}^P m_{ij}^p, \quad \text{and} \quad \frac{1}{m_{ij}^p} = \frac{1}{m_i^p} + \frac{1}{m_j^p}.$$

It is easy to check that one can always find such a decomposition, provided that all the m_{ik} 's are non negative. For instance, a canonical choice is

$$(9) \quad m_{ij} = \sum_{1 \leq k < l \leq n} m_{ij}^{kl},$$

with $m_{ij}^{kl} = \delta_k(i)\delta_l(j)$, where we can write

$$\frac{1}{m_{ij}^{kl}} = \frac{1}{m_i^{kl}} + \frac{1}{m_j^{kl}},$$

where $m_i^{kl} = 2m_{kl}(\delta_k(i) + \delta_l(i))$ for $1 \leq i \leq n$.

We associate to this decomposition a phase field model of the form

$$(10) \quad \partial_t u_k^\varepsilon = m_k^* \left[\sigma_k \left(\Delta u_k^\varepsilon - \frac{1}{\varepsilon^2} W'(u_k^\varepsilon) \right) + \lambda_k^\varepsilon \sqrt{2W(u_k)} \right], \quad \forall k \in \{1, 2, \dots, N\}$$

where we define

- the coefficients m_k^* by

$$m_k^* = \sum_{p=1}^P m_k^p.$$

- the Lagrange multiplier λ_k^ε by

$$\lambda_k^\varepsilon = \frac{1}{m_k^*} \sum_{p=1}^P m_k^p \lambda^{p,\varepsilon}, \quad \text{with} \quad \lambda^{p,\varepsilon} = - \left(\frac{\sum_{k=1}^N m_k^p \sigma_k \left(\Delta u_k^\varepsilon - \frac{1}{\varepsilon^2} W'(u_k^\varepsilon) \right)}{\sum_{k=1}^N m_k^p \sqrt{2W(u_k)}} \right).$$

Remark 1.1. The difference between the two models (7) and (10) lies in the definition of the Lagrange multipliers λ_k^ε . In the first case, the components λ_k^ε are identical and do not differentiate interfaces according to the mobilities for the satisfaction of the constraint $\sum \partial_t u_k = 0$. In the second model, the λ_k^ε 's are weighted in terms of the m_k^p 's.

Remark 1.2. As hinted above, there is, in general, no unique way of decomposing a given set of mobilities $(m_{ij})_{1 \leq i < j \leq N}$ as a sum of harmonically additive mobilities. In view of the tests we performed, it seems that the particular choice of decomposition does not have a strong influence on the numerical results.

Proving the consistency of this new phase field model is the main result of the present work. More precisely, we show that smooth solutions to the above system are close up to order 2 in ε to a sharp interface motion.

Proposition 1.3. Assume that \mathbf{u}^ε is a smooth solution to (10) and define the set

$$E_i^\varepsilon(t) = \{x \in \Omega, \quad u_i^\varepsilon(x, t) \geq 1/2\}$$

and the interface

$$\Gamma_{ij}^\varepsilon(t) = \partial E_i^\varepsilon(t) \cap \{x \in \Omega, \quad u_j^\varepsilon(x, t) \geq u_k^\varepsilon(x, t) \quad \forall k \neq i\}.$$

Then in a neighborhood of Γ_{ij}^ε , \mathbf{u}^ε satisfies

$$\begin{cases} u_i^\varepsilon &= q \left(\frac{d_i^\varepsilon(x, t)}{\varepsilon} \right) + O(\varepsilon^2), \\ u_j^\varepsilon &= 1 - q \left(\frac{d_i^\varepsilon(x, t)}{\varepsilon} \right) + O(\varepsilon^2), \\ u_k^\varepsilon &= O(\varepsilon^2), \text{ for } k \in \{1, 2, \dots, N\} \setminus \{i, j\}, \end{cases}$$

where $d_i^\varepsilon(x, t)$ denotes the signed distance to $E_i^\varepsilon(t)$, with $d_i^\varepsilon(x, t) < 0$ if $x \in E_i^\varepsilon(t)$. Define further $V_{ij}^\varepsilon(x, t) = \partial_t d_i^\varepsilon(x, t)$ for $x \in \Gamma_{ij}$. Then we have the estimate

$$V_{ij}^\varepsilon = m_{ij} \sigma_{ij} H_{ij} + O(\varepsilon).$$

The paper is organized as follows: Proposition 1.3 is proven in Section 2, using the method of matched asymptotic expansions (note that it includes the case of truly harmonically additive mobilities). In Section 3, we propose a numerical scheme based on the phase-field system (10). To illustrate its simplicity, we give an explicit **Matlab** implementation of the scheme in dimension 2, that requires less than 50 lines. In the last section, we provide examples of simulations of multiphase flows in dimension 2 and 3, which illustrate the consistency of the method and the influence of mobilities on the flow.

2. ASYMPTOTIC EXPANSION OF SOLUTIONS TO THE ALLEN-CAHN SYSTEMS

This section is devoted to the formal identification of sharp interface limits of solutions $\mathbf{u}^\varepsilon = (u_1^\varepsilon, \dots, u_N^\varepsilon)$ to the Allen-Cahn systems (10). To this aim, we use the method of matched asymptotic expansions proposed in [15, 29, 6, 24, 13, 12], which we apply around each interface Γ_{ij} . Henceforth, we fix $i, j \in \{1, 2, \dots, N\}$ and we assume that \mathbf{u}^ε is a solution to (10), which is smooth in the vicinity of the interface Γ_{ij}^ε .

2.1. Preliminaries.

Outer expansion far from Γ_{ij}^ε : We assume that the *outer expansion* of u_k^ε , i.e., the expansion far from the front Γ_{ij}^ε has the form:

$$u_k^\varepsilon(x, t) = u_k^0(x, t) + \varepsilon u_k^1(x, t) + O(\varepsilon^2), \text{ for all } k \in \{1, 2, \dots, N\}.$$

In particular and analogously to [24], it is not difficult to see that if $E_i^\varepsilon(t) = \{x \in \Omega, u_i^\varepsilon \geq \frac{1}{2}\}$, then

$$u_i^0(x, t) = \begin{cases} 1 & \text{if } x \in E_i^\varepsilon(t) \\ 0 & \text{otherwise} \end{cases}, \quad u_j^0(x, t) = \begin{cases} 0 & \text{if } x \in E_i^\varepsilon(t) \\ 1 & \text{otherwise} \end{cases}$$

and $u_i^1 = u_j^1 = 0$, $u_k^0 = u_k^1 = 0$ for all $k \in \{1, 2, \dots, N\} \setminus \{i, j\}$.

Inner expansions around Γ_{ij}^ε : In a small neighborhood of Γ_{ij}^ε , we define the stretched normal distance to the front as $z = \frac{1}{\varepsilon} d_i^\varepsilon(x, t)$, where $d_i^\varepsilon(x, t)$ denotes the signed distance to $E_i^\varepsilon(t)$ such that $d_i^\varepsilon(x, t) < 0$ in $E_i^\varepsilon(t)$. The *inner expansions* of $u_k^\varepsilon(x, t)$ and $\lambda^{p,\varepsilon}(x, t)$, i.e. expansions close to the front, are assumed of the form

$$u_k^\varepsilon(x, t) = U_k^\varepsilon(z, x, t) = U_k^0(z, x, t) + \varepsilon U_k^1(z, x, t) + O(\varepsilon^2), \text{ for all } k \in \{1, 2, \dots, N\},$$

and

$$\lambda^{p,\varepsilon}(x, t) = \Lambda^{p,\varepsilon}(z, x, t) = \varepsilon^{-2} \Lambda^{p,-2}(z, x, t) + \varepsilon^{-1} \Lambda^{p,-1}(z, x, t) + O(1).$$

Moreover, if n denotes the unit normal to Γ_{ij} and V_{ij}^ε the normal velocity to the front, for $x \in \Gamma_{ij}$

$$V_{ij}^\varepsilon = \partial_t d_i^\varepsilon(x, t) = V_{ij}^0 + \varepsilon V_{ij}^1 + O(\varepsilon^2), \quad n = \nabla d_i^\varepsilon(x, t).$$

where ∇ refers to the spatial derivative only. Following [29, 24] we assume that $U_k^\varepsilon(z, x, t)$ does not change when x varies normal to Γ_{ij} with z held fixed, or equivalently $(\nabla U_k^\varepsilon)_{z=\text{const.}} \cdot n = 0$. This amounts to requiring that the blow-up with respect to the parameter ε is consistent with the flow.

Following [29, 24], it is easily seen that

$$(11) \quad \begin{cases} \nabla u_k^\varepsilon = \nabla_x U_k^\varepsilon + \varepsilon^{-1} n \partial_z U_k^\varepsilon, \\ \Delta u_k^\varepsilon = \Delta_x U_k^\varepsilon + \varepsilon^{-1} \Delta d_i \partial_z U_k^\varepsilon + \varepsilon^{-2} \partial_{zz}^2 U_k^\varepsilon, \\ \partial_t u_k^\varepsilon = \partial_t U_k^\varepsilon - \varepsilon^{-1} V_{ij}^\varepsilon \partial_z U_k^\varepsilon. \end{cases}$$

Recall also that in a sufficiently small neighborhood of Γ_{ij} , according to Lemma 14.17 in [23], we have

$$\Delta d_i(x, t) = \sum_{k=1}^{d-1} \frac{\kappa_k(\pi(x))}{1 + \kappa_k(\pi(x)) d_i(x, t)} = \sum_{k=1}^{d-1} \frac{\kappa_k(\pi(x))}{1 + \kappa_k(\pi(x)) \varepsilon z},$$

where $\pi(x)$ is the projection of x on Γ_{ij} and κ_k are the principal curvatures on Γ_{ij} . In particular this implies that

$$\Delta d_i^\varepsilon(x, t) = H_{ij} - \varepsilon z \|A_{ij}\|^2 + O(\varepsilon^2),$$

where H_{ij} and $\|A_{ij}\|^2$ denote, respectively, the mean curvature and the squared 2-norm of the second fundamental form of Γ_{ij} at $\pi(x)$.

Matching conditions between outer and inner expansions: The matching conditions (see [24] for more details) can be written as:

$$\lim_{z \rightarrow +\infty} U_i^0(z, x, t) = 0, \quad \lim_{z \rightarrow -\infty} U_i^0(z, x, t) = 1, \quad \lim_{z \rightarrow \pm\infty} U_i^1(z, x, t) = 0,$$

$$\lim_{z \rightarrow +\infty} U_j^0(z, x, t) = 1, \quad \lim_{z \rightarrow -\infty} U_j^0(z, x, t) = 0, \quad \lim_{z \rightarrow \pm\infty} U_j^1(z, x, t) = 0,$$

and

$$\lim_{z \rightarrow \pm\infty} U_k^0(z, x, t) = \lim_{z \rightarrow \pm\infty} U_k^1(z, x, t) = 0, \text{ for all } k \in \{1, 2, \dots, N\} \setminus \{i, j\}.$$

2.2. Analysis of the Allen-Cahn system.

We insert the form (11) in (10) and match the terms according to their powers of ε .

Order ε^{-2} : Identifying the terms of order ε^{-2} gives for all $k \in \{1, \dots, N\}$:

$$\sigma_k (\partial_{zz}^2 U_k^0 - W'(U_k^0)) + \frac{1}{m_k^*} \sum_p m_k^p \Lambda^{p,-2} \sqrt{2W(U_k^0)} = 0,$$

and

$$\left[\sum_{k=1}^N m_k^p \sqrt{2W(U_k^0)} \right] \Lambda^{p,-2} = - \sum_{k=1}^N m_k^p \sigma_k (\partial_{zz}^2 U_k^0 - W'(U_k^0)).$$

This leads to $U_i^0(z, x, t) = q(z)$, $U_j^0(z, x, t) = q(-z)$, $U_k^0(z, x, t) = 0$ for $k \in \{1, 2, \dots, N\} \setminus \{i, j\}$ and $\Lambda^{p,-2} = 0$.

Order ε^{-1} : Matching the next order terms shows that for $k \neq \{1, 2, \dots, N\} \setminus \{i, j\}$,

$$\frac{1}{m_k^*} V_{ij}^0 \partial_z U_k^0 = \sigma_k [\partial_{zz}^2 U_k^1 - W''(U_k^0) U_k^1 + H_{ij} \partial_z U_k^0] + \frac{1}{m_k^*} \sum_p m_k^p \Lambda^{p,-1} \sqrt{2W(U_k^0)}$$

and

$$\left[\sum_{k=1}^N m_k^p \sqrt{2W(U_k^0)} \right] \Lambda^{p,-1} = - \sum_{k=1}^N m_k^p \sigma_k [\partial_{zz}^2 U_k^1 - W''(U_k^0) U_k^1 + H_{ij} \partial_z U_k^0].$$

Notice that for all $k \in \{1, 2, \dots, N\} \setminus \{i, j\}$, we have $m_k \sigma_k (\partial_{zz}^2 U_k^1 - W''(0) U_k^1) = 0$ which, in view of the matching boundary conditions, yields $U_k^1 = 0$.

Moreover, recalling from (2) that $\sqrt{2W(q)} = -q'$, the equations for U_i^1 and $\Lambda^{p,-1}$ become

$$V_{ij}^0 q'(z) = \sigma_i m_i^* (\partial_{zz}^2 U_i^1 - W''(q(z)) U_i^1) + \sigma_i q'(z) H_{ij} - \sum_p m_i^p \Lambda^{p,-1}(z, x, t) q'(z),$$

and

$$\begin{aligned} (m_i^p + m_j^p) q'(z) \Lambda^{p,-1}(z, x, t) &= m_i^p \sigma_i (\partial_{zz}^2 U_i^1 - W''(q(z)) U_i^1) + m_i^p \sigma_i q'(z) H_{ij} + \\ &+ m_j^p \sigma_j (\partial_{zz}^2 U_j^1 - W''(q(z)) U_j^1) - m_j^p \sigma_j q'(z) H_{ij}. \end{aligned}$$

In particular this last equation shows that

$$\begin{aligned} \sum_p [m_i^p \Lambda^{p,-1}(z, x, t) q'(z)] &= \left(\sum_p \frac{m_i^p}{m_j^p} m_{ij}^p \right) [\sigma_i (\partial_{zz}^2 U_i^1 - W''(q(z)) U_i^1) + \sigma_i q'(z) H_{ij}] \\ &\quad + \left(\sum_p m_{ij}^p \right) [\sigma_j (\partial_{zz}^2 U_j^1 - W''(q(z)) U_j^1) - \sigma_j q'(z) H_{ij}]. \end{aligned}$$

as $m_{ij}^p = \frac{m_i^p m_j^p}{m_i^p + m_j^p}$. Then

$$\begin{aligned} V_{ij}^0 q'(z) &= \left[\left(m_i^* - \sum_p \frac{m_i^p}{m_j^p} m_{ij}^p \right) \sigma_i + \left(\sum_p m_{ij}^p \right) \sigma_j \right] q'(z) H_{ij} \\ &\quad + \left(m_i^* - \sum_p \frac{m_i^p}{m_j^p} m_{ij}^p \right) \sigma_i (\partial_{zz}^2 U_i^1 - W''(q(z)) U_i^1) \\ &\quad - \left(\sum_p m_{ij}^p \right) \sigma_j (\partial_{zz}^2 U_j^1 - W''(q(z)) U_j^1). \end{aligned}$$

Moreover, remarking that

$$\left(m_i^* - \sum_p \frac{m_i^p}{m_j^p} m_{ij}^p \right) = \sum_p m_{ij}^p = m_{ij},$$

we deduce that U_i^1, U_j^1 and V_{ij}^0 satisfy

$$V_{ij}^0 q'(z) = \sigma_{i,j} m_{ij} q'(z) H_{ij} + m_{ij} \sigma_i (\partial_{zz}^2 U_i^1 - W''(q(z)) U_i^1) - m_{ij} \sigma_j (\partial_{zz}^2 U_j^1 - W''(q(z)) U_j^1).$$

Multiplying this equation by q' and integrating over \mathbb{R} leads to the interface evolution

$$V_{ij}^0 = m_{ij} \sigma_{i,j} H_{ij},$$

and $\sigma_i U_i^1 - \sigma_j U_j^1 = 0$. We then deduce that $U_i^1 = U_j^1 = 0$ by using the partition constraint $\sum_{k=1}^N U_k^1 = U_i^1 + U_j^1 = 0$. Moreover, we have

$$\left(m_i^p + m_j^p \right) q'(z) \Lambda^{p,-1}(z, x, t) = m_i^p \sigma_i q'(z) H_{ij}(x) - m_j^p \sigma_j q'(z) H_{ij}(x),$$

which shows that

$$\Lambda^{p,-1} = \left(\frac{m_{i,j}^p}{m_i^p} \sigma_i - \frac{m_{i,j}^p}{m_j^p} \sigma_j \right) H_{i,j},$$

and finally proves proposition 1.3.

3. NUMERICAL SCHEME AND IMPLEMENTATION

In this section we introduce a Fourier spectral splitting scheme [17] to approximate the solutions to the following Allen-Cahn system:

$$\partial_t u_k^\varepsilon = m_k^* \left[\sigma_k \left(\Delta u_k^\varepsilon - \frac{1}{\varepsilon^2} W'(u_k^\varepsilon) \right) + \lambda_k^\varepsilon \sqrt{2W(u_k)} \right],$$

for all $k \in \{1, 2, \dots, N\}$ where $m_k^* = \sum_{p=1}^P m_k^p$ and

$$\lambda_k^\varepsilon = \frac{1}{m_k^*} \sum_{p=1}^P m_k^p \lambda^{p,\varepsilon}, \quad \text{with} \quad \lambda^{p,\varepsilon} = - \left(\frac{\sum_{k=1}^N m_k^p \sigma_k \left(\Delta u_k^\varepsilon - \frac{1}{\varepsilon^2} W'(u_k^\varepsilon) \right)}{\sum_{k=1}^N m_k^p \sqrt{2W(u_k)}} \right).$$

More precisely, this system is solved on a square-box $Q = [0, L_1] \times \dots \times [0, L_d]$ with periodic boundary conditions.

We recall that the Fourier K -approximation of a function u defined in a box Q is given by

$$u^K(x) = \sum_{\mathbf{k} \in K_d} c_{\mathbf{k}} e^{2i\pi \xi_{\mathbf{k}} \cdot x},$$

where $K_d = [-\frac{K_1}{2}, \frac{K_1}{2} - 1] \times [-\frac{K_2}{2}, \frac{K_2}{2} - 1] \cdots \times [-\frac{K_d}{2}, \frac{K_d}{2} - 1]$, $\mathbf{k} = (k_1, \dots, k_d)$ and $\xi_{\mathbf{k}} = (k_1/L_1, \dots, k_d/L_d)$. In this formula, the $c_{\mathbf{k}}$'s denote the K^d first discrete Fourier coefficients of u . The inverse discrete Fourier transform leads to $u_{\mathbf{k}}^K = \text{IFFT}[c_{\mathbf{k}}]$ where $u_{\mathbf{k}}^K$ denotes the value of u at the points $x_{\mathbf{k}} = (k_1 h_1, \dots, k_d h_d)$ and where $h_i = L_i/N_i$ for $i \in \{1, \dots, d\}$. Conversely, $c_{\mathbf{k}}$ can be computed as the discrete Fourier transform of $u_{\mathbf{k}}^K$, *i.e.*, $c_{\mathbf{k}} = \text{FFT}[u_{\mathbf{k}}^K]$.

3.1. Definition of the scheme.

Given a time discretisation parameter $\delta_t > 0$, we construct a sequence $(\mathbf{u}^n)_{n \geq 0}$ of approximations of \mathbf{u} at the times $n\delta_t$, using a splitting method as in [13, 12]. Iteratively we

- minimize the Cahn Hillard energy without the constraint $\sum_{k=1}^N u_k^n = 1$.
- compute the contribution of the Lagrange multipliers λ_k^ε and update the values of u_k^n .

This algorithm provides a simple scheme, and our numerical experiments (see Section 4) indicate that it is efficient, stable and that it preserves the partition constraint in the sense that

$$\sum_{k=1}^N u_k^{n+1} = \sum_{k=1}^N u_k^0, \quad \forall n \in \mathbb{N}.$$

Step 1: The decoupled Allen Cahn system without the partition constraint :

Let $\mathbf{u}^{n+1/2}$ denote an approximation of $\mathbf{v}(\delta_t)$, where $\mathbf{v} = (v_1, \dots, v_N)$ is the solution with periodic boundary conditions on ∂Q to:

$$\begin{cases} \partial_t v_k(x, t) &= m_k^* \sigma_k [\Delta v_k(x, t) - \frac{1}{\varepsilon^2} W'(v_k(x, t))], & (x, t) \in Q \times [0, \delta_t], \\ \mathbf{v}(x, 0) &= \mathbf{u}^n(x), & x \in Q. \end{cases}$$

Here, our motivation is to introduce a stable scheme in the sense that the associated Cahn Hillard energy decreases with the iterations. A totally implicit scheme would require the resolution of a nonlinear system at each iteration, which in practice would prove costly and not very accurate. Rather, we opted for a semi-implicit scheme, in which the non linear term $W'(v_k)$ is integrated explicitly. More precisely, we consider the following scheme

$$(I_d - \delta_t m_k^* \sigma_k (\Delta - \alpha/\varepsilon^2 I_d)) u_k^{n+1/2} = u_k^n - \frac{\delta_t m_k^* \sigma_k}{\varepsilon^2} (W'(u_k^n) - \alpha u_k^n),$$

where α is a positive stabilization parameter, chosen sufficiently large to ensure the stability of the scheme. Indeed, it is known that the Cahn-Hilliard energy decreases unconditionally as soon as the explicit part, *i.e.*, $s \rightarrow W'(s) - \alpha s$ is the derivative of a concave function [19, 31]. This is the case for the potential $W(s) = \frac{1}{2} s^2 (1 - s)^2$, as soon as $\alpha > 2$. We also note that even when $\alpha = 0$, the semi-implicit scheme is stable under the classical condition $\delta_t \leq \frac{C}{\varepsilon^2}$, where $C = \sum_{s \in [0, 1]} |W''(s)|$. Further, as the fields u_k^n are required to satisfy periodic boundary conditions on ∂Q , the action of the inverse operator $(I_d - m_k \delta_k \delta_t (\Delta - \alpha/\varepsilon^2 I_d))^{-1}$ is easily computed in Fourier space [17] using the Fast Fourier Transform. Finally, this strategy can also be generalized to anisotropic flows [9].

Step 2: Explicit projection onto the partition constraint $\sum u_k = 1$.

The advantage of an implicit treatment of the Lagrange multiplier λ_k^ε is not sufficiently interesting with respect to the complexity and the algorithmic cost of a such approach. We then prefer an explicit approach for which, the treatment appears exact in the sense

that $\sum_{k=1}^N u_k^{n+1} = \sum_{k=1}^N u_k^n$, $\forall n \in \mathbb{N}$. More precisely, for all $k \in \{1, 2, \dots, N\}$, we define u_k^{n+1} by

$$u_k^{n+1} = u_k^{n+1/2} + \delta_t m_k^* \lambda_k^{n+1/2} \sqrt{2W(u_k^{n+1/2})}$$

where

$$\lambda_k^{n+1/2} = \frac{1}{m_k^*} \sum_{p=1}^P m_k^p \lambda^{p,n+1/2},$$

and

$$\lambda^{p,n+1/2} = \begin{cases} -\frac{\sum_{i=1}^N m_i^p \alpha_i^{n+1/2}}{\sum_{i=1}^N m_i^p \sqrt{2W(u_i^{n+1/2})}} & \text{if } \sum_i m_i^p > 0 \\ 0 & \text{otherwise} \end{cases}.$$

Here $\alpha_i^{n+1/2}$ is a semi-implicit approximation of $\sigma_i [\Delta u_i(x, t) - \frac{1}{\varepsilon^2} W'(u_i(x, t))]$ at the time $t_{n+1/2}$ and is defined by

$$\alpha_i^{n+1/2} = \frac{u_i^{n+1/2} - u_i^n}{\delta_t m_i^*}.$$

Remark 3.1. The previous definitions of $\alpha_i^{n+1/2}$ and $\lambda_k^{n+1/2}$ only make sense when the m_i^* 's or the sum $\sum_{i=1}^N m_i^p \sqrt{2W(u_i^{n+1/2})}$ do not vanish. In practice, (see figure (1)) to overcome this difficulty and avoid any division by zero, we use the following regularized version of the scheme :

$$u_k^{n+1} = u_k^{n+1/2} + \delta_t \tilde{\lambda}_k^{n+1/2} \left(\sqrt{2W(u_k^{n+1/2})} + \beta \right), \quad \tilde{\lambda}_k^{n+1/2} = \sum_{p=1}^P m_k^p \tilde{\lambda}^{p,n+1/2},$$

$$\tilde{\lambda}^{p,n+1/2} = \begin{cases} -\frac{\sum_{i=1}^N m_i^p \alpha_i^{n+1/2}}{\sum_{i=1}^N m_i^p (\sqrt{2W(u_i^{n+1/2})} + \beta)} & \text{if } \sum_i m_i^p > 0, \\ 0 & \text{otherwise} \end{cases},$$

and

$$\tilde{\alpha}_i^{n+1/2} = \frac{u_i^{n+1/2} - u_i^n}{\delta_t \max\{m_i^*, \beta\}},$$

where β is the machine epsilon number $\beta \simeq 1.110^{-16}$.

Proposition 3.2.

(1) Assume that $m_i^* > \beta$ for all $i \in \{1, \dots, N\}$ and $\sum_i m_i^p > 0$ for all $p \in \{1, \dots, P\}$, then the previous scheme preserves the partition constraint, i.e.

$$\sum_{k=1}^N u_k^{n+1} = \sum_{k=1}^N u_k^n.$$

(2) Assume that $m_{ij} = 0$ for all $j \in \{1, 2, \dots, N\}$, then

$$u_i^{n+1} = u_i^n.$$

Proof of (1) : As

$$u_k^{n+1} = u_k^{n+1/2} - \sum_{p=1}^P m_k^p \left[\frac{\sum_{i=1}^N m_i^p (u_i^{n+1/2} - u_i^n) / \max\{m_i^*, \beta\}}{\sum_{i=1}^N m_i^p (\sqrt{2W(u_i^{n+1/2})} + \beta)} \right] (\sqrt{2W(u_k^{n+1/2})} + \beta)$$

it follows that

$$\begin{aligned} \sum_{k=1}^N u_k^{n+1} &= \sum_{k=1}^N u_k^{n+1/2} - \sum_{p=1}^P \left[\sum_{i=1}^N m_i^p (u_i^{n+1/2} - u_i^n) / m_i^* \right] \frac{\sum_{k=1}^N m_k^p (\sqrt{2W(u_k^{n+1/2})} + \beta)}{\sum_{i=1}^N m_i^p (\sqrt{2W(u_i^{n+1/2})} + \beta)} \\ &= \sum_{k=1}^N u_k^{n+1/2} - \sum_{i=1}^N (u_i^{n+1/2} - u_i^n) \sum_{p=1}^P m_i^p / m_i^* = \sum_{k=1}^N u_k^n. \end{aligned}$$

Proof of (2) : Recall that $\sum_p m_{ij}^p = m_{ij}$ with $m_{i,j} = 0$. We then deduce that $m_{ij}^p = 0$ for all $p \in \{1, 2, \dots, P\}$ as these coefficients are all non negatives. Moreover, as the mobility coefficient m_{ij}^p is harmonically additive i.e

$$m_{ij}^p = (1/m_i^p + 1/m_j^p)^{-1},$$

we then deduce that $m_i^p = 0$ for all $p \in \{1, 2, \dots, P\}$ and $m_i^* = \sum_p m_i^p = 0$. Finally, the first step gives $u_i^{n+1/2} = u_i^n$ as $m_i^* = 0$ and the second step gives $\tilde{\lambda}_i^{n+1/2} = \sum_{p=1}^P m_i^p \tilde{\lambda}_i^p = 0$ and $u_i^{n+1} = u_i^{n+1/2} = u_i^n$ as $\tilde{\lambda}^{p,n+1/2}$ is bounded and $m_i^p = 0$ for all $p \in \{1, \dots, P\}$.

3.2. Matlab code.

We present in the following figure an example of **Matlab** code with less than 50 lines which implements the previous scheme in the case of $N = 3$ phases. In particular :

- The lines 3 to 10 correspond to initialization of the phase u_k for $k = 1 : 3$.
- The lines 15 to 21 corresponds to the following canonical decomposition of the mobility coefficients m_{ij} :

$$\begin{aligned} (m_{12}, m_{13}, m_{23}) &= (m_{12}^1, m_{13}^1, m_{23}^1) + (m_{12}^2, m_{13}^2, m_{23}^2) + (m_{12}^3, m_{13}^3, m_{23}^3) \\ &= (m_{12}, 0, 0) + (0, m_{13}, 0) + (0, 0, m_{23}) \end{aligned}$$

- The lines 24 to 28 corresponds to the operator associated to numerical resolution of the equation

$$(I_d - \delta_t m_k^* \sigma_k (\Delta - \alpha/\varepsilon^2 I_d)) u_k^{n+1/2} = u_k^n - \frac{\delta_t m_k^* \sigma_k}{\varepsilon^2} (W'(u_k^n) - \alpha u_k^n),$$

More precisely, the operators OP and OL are respectively theoretical defined by

$$OP(u) = u - \frac{\delta_t m \sigma}{\varepsilon^2} (W'(u) - \alpha u) \text{ and } OL(u) = (I_d - \delta_t m \sigma (\Delta - \alpha/\varepsilon^2 I_d))^{-1} u$$

- Lines 38-40 corresponds to the computation of each Lagrange multipliers $\lambda^{p,n+1/2}$.

4. NUMERICAL EXPERIMENTS AND VALIDATION

In this section, we report numerical experiments in dimension $d = 2$ and $d = 3$ with $N = 3$ or $N = 4$ phases. In each case, the computational domain Q is a cube $[-0.5, 0.5]^d$ of size 1 discretized with $K = 2^8$ nodes in 2D and $K = 2^7$ in 3D, in each direction. We also use the classical double well potential $W(s) = \frac{1}{2}s^2(1-s)^2$.

4.1. Validation of the consistency of our approach.

This first test illustrates the consistency of the numerical scheme in the case of $N = 3$ phases. We consider the evolution of two circles by the flow (10) associated to the following surface tensions and mobilities

$$(\sigma_{12}, \sigma_{13}, \sigma_{23}) = (1, 1, 1) \text{ and } (m_{12}, m_{13}, m_{23}) = (1, 1, 0.25).$$

Notice that as explained previously, this set of mobilities is not harmonically additive. More precisely, the initial sets are chosen in the following way:

- the phase u_1 fills a circle of radius $r_1 = 0.2$ centered at $x = (-0.25, 0, 0)$

```

1  %%%%%%%%% Resolution parameters
2  N = 2^8; epsilon = 1/N; dt = 10/N^2; L = 1; T = 1;
3
4  %%%%%%%%% initial condition %%%%%%%%%
5  x = linspace(-L/2,L/2,N); [Y,X] = meshgrid(x,x); R = 0.3;
6  d1 = max(sqrt((X).^2 + (Y + 0.1).^2) - R, Y - 0.05*cos(12*pi*X)); U1 = 1/2 - 1/2*(tanh(d1/epsilon/2));
7  d2 = max(sqrt((X).^2 + (Y - 0.1).^2) - R, -Y + 0.05*cos(12*pi*X)); U2 = (1/2 - 1/2*(tanh(d2/epsilon/2)));
8  U3 = 1 - (U1 + U2);
9
10 %%%%%%%%% surface and mobility coefficients %%%%%%%%%
11 sigma12 = 1; sigma13 = 1; sigma23 = 1; m12 = 1; m13 = 0; m23 = 0;
12
13 %%%%%%%%% coefficients m_{i,j}^p and m_{i}^p %%%%%%%%%
14 sigma1 = (sigma12 + sigma13 - sigma23)/2; sigma2 = (sigma12 + sigma23 - sigma13)/2; sigma3 = (sigma23 +
    sigma13 - sigma12)/2;
15 m12_1 = m12; m13_1 = 0; m23_1 = 0; m1_1 = 2*m12; m2_1 = 2*m12; m3_1 = 0;
16 m12_2 = 0; m13_2 = m13; m23_2 = 0; m1_2 = 2*m13; m2_2 = 0; m3_2 = 2*m13;
17 m12_3 = 0; m13_3 = 0; m23_3 = m23; m1_3 = 0; m2_3 = 2*m23; m3_3 = 2*m23;
18 m1 = m1_1 + m1_2 + m1_3; m2 = m2_1 + m2_2 + m2_3; m3 = m3_1 + m3_2 + m3_3;
19 %%%%%%%%% Diffusion and reaction operators
20 k = [0:N/2,-N/2+1:-1]; [K1,K2] = meshgrid(k,k); Delta = (K1.^2 + K2.^2);
21 sqrtWU = @(U) abs(U.*(1-U)); potentiel_prim = @(U) U.*(1-U).*(1 - 2*U);
22 alpha = 2;
23 OP = @(U,dt,epsilon,sigma,m,alpha) U - dt/epsilon^2*sigma*m*(potentiel_prim(U) - alpha*U);
24 OL = @(U,dt,epsilon,sigma,m,alpha) ifft2((1./(1 + dt*m*sigma*(4*pi^2*Delta + alpha/epsilon^2))).*fft2(U));
25
26 %%%%%%%%% Computation of the solution %%%%%%%%%
27 for n=1:T/dt,
28 %%%%%%%%% Step 1 % Cahn Hilliard flow
29 U1_p = OL(OP(U1,dt,epsilon,sigma1,m1,alpha),dt,epsilon,sigma1,m1,alpha);
30 U2_p = OL(OP(U2,dt,epsilon,sigma2,m2,alpha),dt,epsilon,sigma2,m2,alpha);
31 U3_p = OL(OP(U3,dt,epsilon,sigma3,m3,alpha),dt,epsilon,sigma3,m3,alpha);
32 %%%%%%%%% Step 2 % Lagrange multiplier Lambda
33 alpha1 = (U1_p - U1)/(dt*max(m1,eps)); alpha2 = (U2_p - U2)/(dt*max(m2,eps)); alpha3 = (U3_p - U3)/(dt*max(
    m3,eps));
34 if (m1_1 + m2_1 + m3_1>0), lambda_p1 = - ( m1_1*alpha1 + m2_1*alpha2 + m3_1*alpha3)/(m1_1*(sqrtWU(U1_p)+
    eps) + m2_1*(sqrtWU(U2_p)+eps) + m3_1*(sqrtWU(U3_p)+eps));
35 else lambda_p1 = 0; end
36 if ( m1_2 + m2_2 + m3_2>0), lambda_p2 = - ( m1_2*alpha1 + m2_2*alpha2 + m3_2*alpha3)/(m1_2*(sqrtWU(U1_p)+
    eps) + m2_2*(sqrtWU(U2_p)+eps) + m3_2*(sqrtWU(U3_p)+eps));
37 else lambda_p2 = 0; end
38 if ( m1_3 + m2_3 + m3_3>0), lambda_p3 = - ( m1_3*alpha1 + m2_3*alpha2 + m3_3*alpha3)/(m1_3*(sqrtWU(U1_p)+
    eps) + m2_3*(sqrtWU(U2_p)+eps) + m3_3*(sqrtWU(U3_p)+eps));
39 else lambda_p3 = 0; end
40
41 U1 = U1_p + dt*(m1_1*lambda_p1 + m1_2*lambda_p2 + m1_3*lambda_p3).*(sqrtWU(U1_p)+eps);
42 U2 = U2_p + dt*(m2_1*lambda_p1 + m2_2*lambda_p2 + m2_3*lambda_p3).*(sqrtWU(U2_p)+eps);
43 U3 = U3_p + dt*(m3_1*lambda_p1 + m3_2*lambda_p2 + m3_3*lambda_p3).*(sqrtWU(U3_p)+eps);
44
45 if (mod(n,10)==1)
46     imagesc(U3 + 2*U2)
47     pause(0.01);
48 end
49 end

```

FIGURE 1. Example of **Matlab** implementation of the previous scheme in the case of $N = 3$ phases in dimension 2.

- the phase u_2 fills a circle of radius $r_2 = 0.2$ centered at $x = (0.25, 0, 0)$

In particular, each of these sets should evolve as a circle, with radius satisfying

$$R_1(t) = \sqrt{r_1^2 - 2\sigma_{13}m_{13}t} \text{ and } R_2(t) = \sqrt{r_2^2 - 2\sigma_{23}m_{23}t}.$$

The following parameters have been used in the computations: $\varepsilon = 1.5/K$, $\delta_t = 0.25/K^2$ and $\alpha = 0$. Figure (2) represents the multiphase solution $\mathbf{u}^\varepsilon = (u_1^\varepsilon, u_2^\varepsilon, u_3^\varepsilon)$ at different times. The first picture in Figure (3) shows a very good agreement between the approximative radii R_1^ε and R_2^ε and their expected theoretical values. The second picture in Figure (3) shows that the numerical error on the constraint $\sum_k u_k = 1$ is of the order of 10^{-12} in this context.

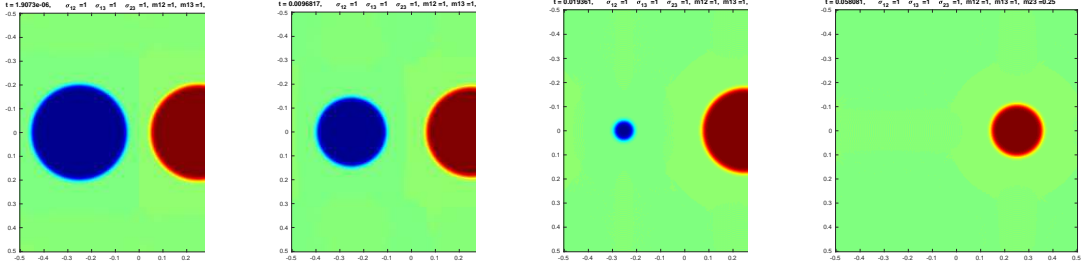


FIGURE 2. Mean curvature flow of two circles, with $\sigma_{12} = \sigma_{13} = \sigma_{23} = 1$ and $m_{12} = 1$, $m_{13} = 1$ and $m_{23} = 0.25$. Plots of the function $2u_2 + u_3$ at different times : u_1 , u_2 and u_3 are represented in blue, red and green respectively.

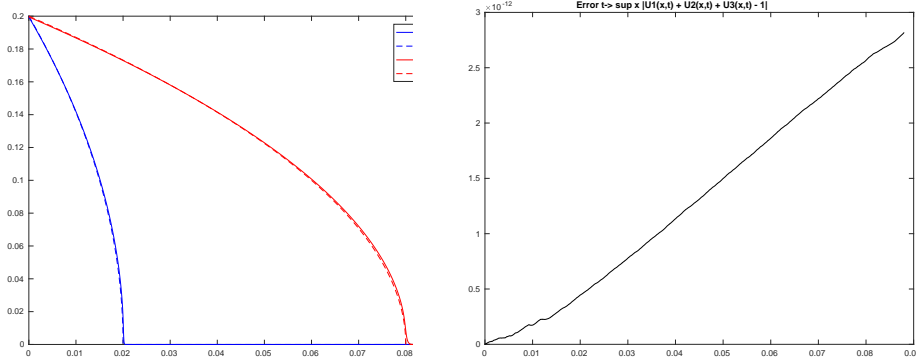


FIGURE 3. Mean curvature flow of two circles. Identical surface tensions, $(m_{12}, m_{13}, m_{23}) = (1, 1, 0.25)$. Left : Comparison of the radii $R_k^\varepsilon(t)$ and their theoretical values $R_k(t)$ associated with the phases u_k , $k=1,2$. Right: Plot of $\|1 - \sum_k u_k(\cdot, t)\|_{L^\infty}$

4.2. Influence of the choice of mobilities decomposition.

The decomposition (8) is not unique and it is therefore legitimate to question its effect on the numerical approximation of the flow. We consider here the simplest case using $N = 3$ phases, homogeneous surface tensions $\sigma_{i,j} = 1$ and homogeneous mobility coefficients $m_{ij} = 1$. We then compare the numerical approximations associated with the following decomposition of the mobilities :

- the canonical choice

$$(m_{12}, m_{13}, m_{23}) = (m_{12}, 0, 0) + (0, m_{13}, 0) + (0, 0, m_{23}),$$

with

$$(m_{12}, m_{13}, m_{23}) = (1, 1, 1) = (1, 0, 0) + (0, 1, 0) + (0, 0, 1).$$

- a sparse decomposition

$$(m_{12}, m_{13}, m_{23}) = (1, 1, 1) = (1, 1, 1) + (0, 0, 0) + (0, 0, 0),$$

(notice that $(m_{12}, m_{13}, m_{23}) = (1, 1, 1)$ is indeed harmonically additive).

The following numerical parameters $\varepsilon = 1.5/K$, $\delta_t = 0.25/K^2$ and $\alpha = 0$ have been used. Figure (4) shows the multiphase solution $\mathbf{u}^\varepsilon = (u_1^\varepsilon, u_2^\varepsilon, u_3^\varepsilon)$ at different times. The rows correspond to the canonical and sparse decomposition of the m_{ij} 's respectively . We observe that the two flows are quite similar, which shows the little influence of the choice of decomposition.

4.3. Validation of our approach for highly contrasted mobilities.

Our next tests show that our approach can handle highly contrasted mobilities. One expects that when m_{ij} is small (or vanishes) the corresponding interface Γ_{ij} hardly moves. The tests

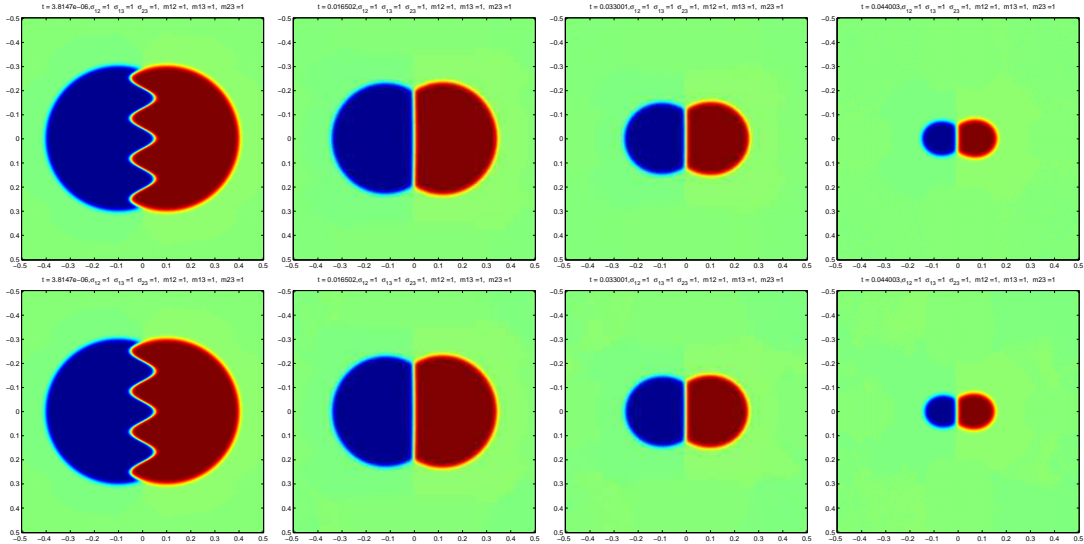


FIGURE 4. Influence of the choice of decomposition of the mobilities : the canonical (first row) and the sparse decomposition (second row) of the mobility coefficients. The pictures represent the graphs of $2u_2 + u_3$ at different times, u_1 , u_2 and u_3 are depicted in blue, red and green respectively.

also show that mobilities are parameters that may strongly affect the flow. The computations have been performed with $\varepsilon = 1/K$, $\delta_t = 1/K^2$ and $\alpha = 2$. Figure (5) represents a first series of numerical experiments in which $\sigma_{12} = \sigma_{13} = \sigma_{23} = 1$. The rows depict the flow associated with the mobilities $(m_{12}, m_{13}, m_{23}) = (1, 1, 1)$, $(0, 1, 1)$ and $(0, 1, 0)$ respectively, with the same initial condition. On each graph, the phases u_1 and u_2 are plotted in blue and red respectively. One can observe that, as expected, the blue-red interface Γ_{12} does not move when $m_{12} = 0$ (second line), or when m_{23} (third line).

Figures (6) represent similar experiments with the non-identical surface tensions $\sigma_{12} = 0.1$ and $\sigma_{13} = \sigma_{23} = 1$. The same conclusions hold.

4.4. Numerical experiments with $N = 4$ phases. We show here that our method can handle flows involving more than 3 phases (recall that the mobilities associated with 3 phases are always harmonically additive). Here we consider 4 phases and a canonical decomposition of the mobilities $\mathbf{m} = (m_{12}, m_{13}, m_{14}, m_{23}, m_{24}, m_{34})$, which takes the form

$$(m_{12}, m_{13}, m_{14}, m_{23}, m_{24}, m_{34}) = \sum_{p=1}^6 (m_{12}^p, m_{13}^p, m_{14}^p, m_{23}^p, m_{24}^p, m_{34}^p),$$

where

$$(m_{12}^p, m_{13}^p, m_{14}^p, m_{23}^p, m_{24}^p, m_{34}^p) = \begin{cases} (m_{12}, 0, 0, 0, 0, 0) & \text{if } p = 1 \\ (0, m_{13}, 0, 0, 0, 0) & \text{if } p = 2 \\ \vdots & \\ (0, 0, 0, 0, 0, m_{34}) & \text{if } p = 6 \end{cases}$$

Figure (7) shows a series of numerical experiments using

$$(\sigma_{12}, \sigma_{13}, \sigma_{14}, \sigma_{23}, \sigma_{24}, \sigma_{34}) = (1, 1, 1, 1, 1, 1).$$

The rows correspond to $\mathbf{m} = (1, 1, 1, 1, 1, 1)$, $\mathbf{m} = (0, 1, 1, 1, 1, 1)$ and $\mathbf{m} = (0, 0, 1, 1, 1, 1)$ respectively. In particular, in each graph, the phases u_1, u_2, u_3, u_4 are depicted in light blue, red, blue and green respectively. These results show good agreement with the expected theoretical flows.

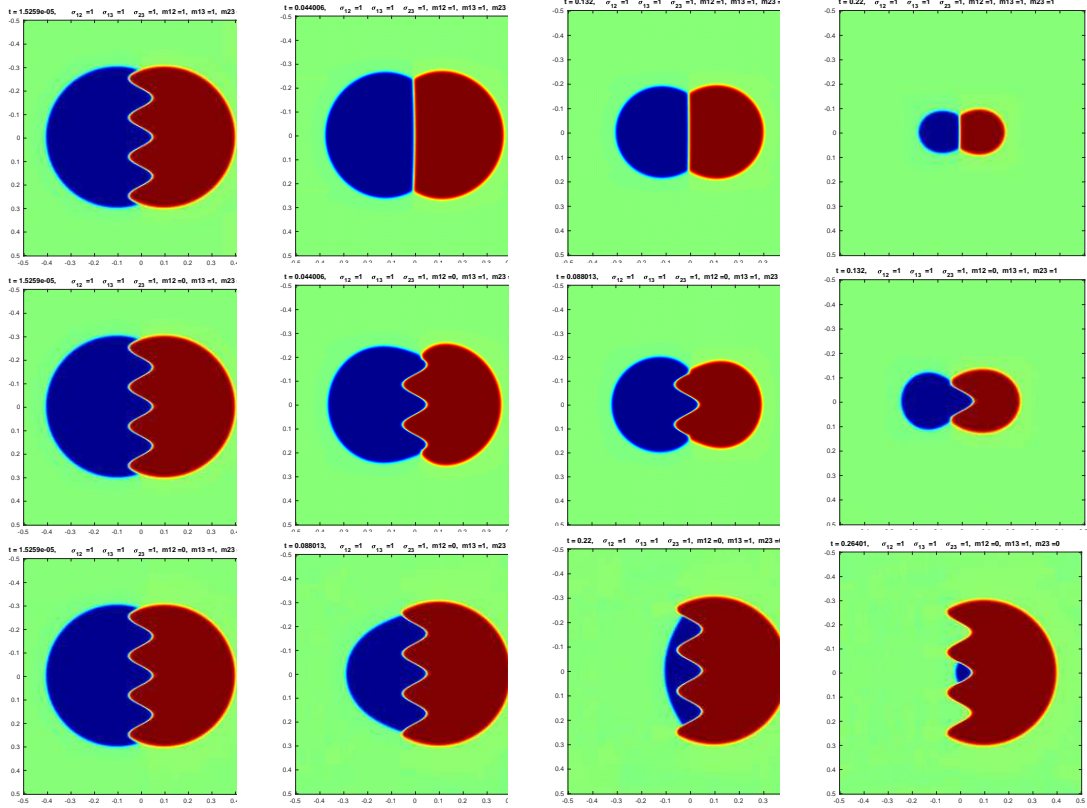


FIGURE 5. Mean curvature flows with high contrast mobilities, identical surface tensions. The rows correspond to $(m_{12}, m_{13}, m_{23}) = (1, 1, 1)$, $(m_{12}, m_{13}, m_{23}) = (0, 1, 1)$ and $(m_{12}, m_{13}, m_{23}) = (0, 1, 0)$ respectively. We plot in each picture the value of the function $2u_2 + u_3$ at different time t where u_1 , u_2 and u_3 appear respectively in blue, red and green.

4.5. Numerical experiments in dimension 3.

Figure (8) represents the 3D version of the 2D computations reported in Figure (5). The surface tensions are identical, $\sigma_{ij} = 1$. The row represent evolutions from the same initial conditions, with mobilities (m_{12}, m_{13}, m_{23}) equal to $(1, 1, 1)$, $(0, 1, 1)$ and $(0, 1, 0)$ respectively. In each graph, the phases u_1 and u_2 are depicted in blue and red, respectively.

Our last example, shown in Figure (8), concerns a more complex situation with 3 phases, where the initial geometry represents a toy truck. We compare evolutions obtained with different sets of mobilities, and where the surface tensions $\sigma_{i,j}$ are all equal to 1.

5. CONCLUSION

We propose a numerical scheme for multiphase mean curvature flow with general mobilities. The scheme uses a decomposition of the set of mobilities as sums of harmonically additive mobilities. We perform a formal asymptotic expansion that shows that smooth solutions of the associated Allen-Cahn equation approximate a sharp interface motion driven by $V_{ij} = m_{i,j}\sigma_{ij}H_{ij}$, $1 \leq i < j \leq N$, up to order 2 in the order parameter ε . The numerical tests we report are consistent with this expected accuracy. In particular, when the contrast between mobilities is large, our scheme generates approximate flows where the width of the diffuse interface between phases is not affected by that mobility contrast.

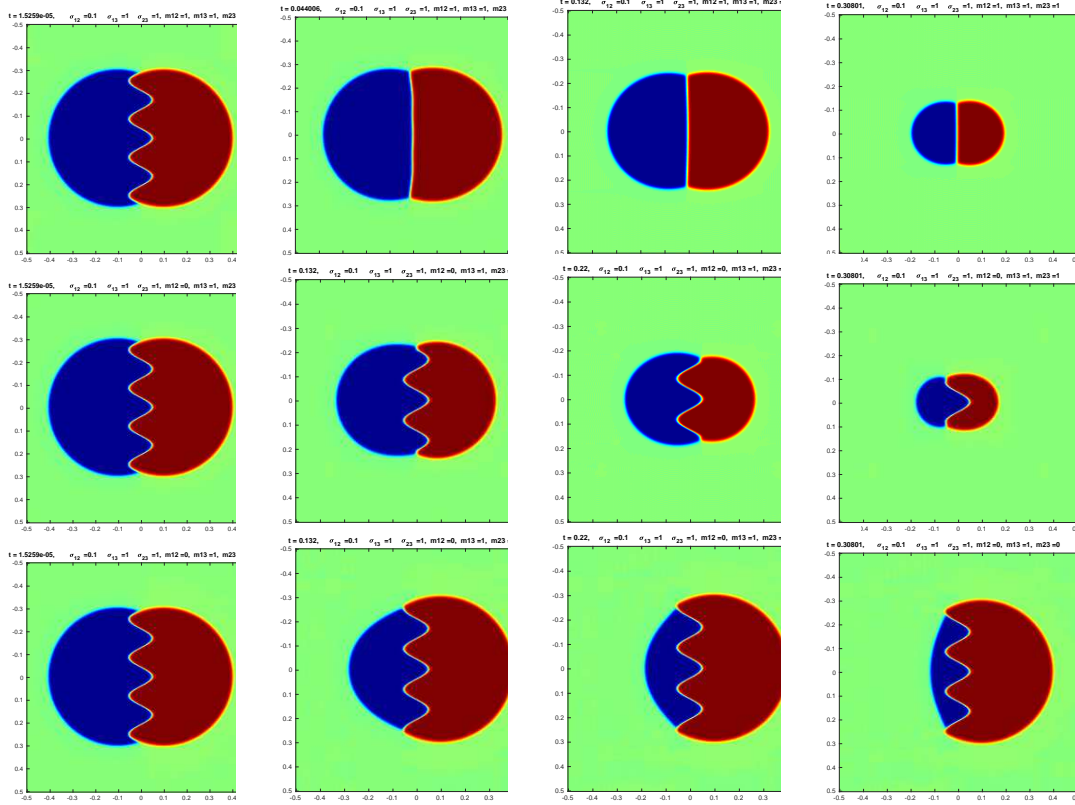


FIGURE 6. Mean curvature flows with high contrast mobilities, non-identical surface tensions. The rows correspond to $(m_{12}, m_{13}, m_{23}) = (1, 1, 1)$, $(m_{12}, m_{13}, m_{23}) = (0, 1, 1)$ and $(m_{12}, m_{13}, m_{23}) = (0, 1, 0)$ respectively. We plot in each pictures the value of the function $2u_2 + u_3$ at different time t where u_1 , u_2 and u_3 appear respectively in blue, red and green.

ACKNOWLEDGMENT

The authors acknowledge support from the French National Research Agency (ANR) under grants ANR-18-CE05-0017 (project BEEP) and ANR-19-CE01-0009-01 (project MIMESIS-3D). Part of this work was also supported by the LABEX MILYON (ANR-10-LABX-0070) of Université de Lyon, within the program "Investissements d'Avenir" (ANR-11-IDEX-0007) operated by the French National Research Agency (ANR).

REFERENCES

- [1] Allen, S.M., Cahn, J.W.: A microscopic theory for antiphase boundary motion and its application to antiphase domain coarsening. *Acta Metall.* **27**, 1085–1095 (1979) [2](#)
- [2] Ambrosio, L.: Geometric evolution problems, distance function and viscosity solutions. In: *Calculus of variations and partial differential equations* (Pisa, 1996), pp. 5–93. Springer, Berlin (2000) [2](#)
- [3] Baldo, S.: Minimal interface criterion for phase transitions in mixtures of cahn-hilliard fluids. *Annales de l'institut Henri Poincaré (C) Analyse non linéaire* **7**(2), 67–90 (1990). URL <http://eudml.org/doc/782163> [3](#)
- [4] Bellettini, G.: *Lecture Notes on Mean Curvature Flow, Barriers and Singular Perturbations*. Scuola Normale Superiore, Pisa (2013) [2](#)
- [5] Bellettini, G., Paolini, M.: Quasi-optimal error estimates for the mean curvature flow with a forcing term. *Differential Integral Equations* **8**(4), 735–752 (1995) [2](#)
- [6] Bellettini, G., Paolini, M.: Quasi-optimal error estimates for the mean curvature flow with a forcing term. *Differential Integral Equations* **8**(4), 735–752 (1995) [6](#)
- [7] Ben Said, M., Selzer, M., Nestler, B., Braun, D., Greiner, C., Garcke, H.: A phase-field approach for wetting phenomena of multiphase droplets on solid surfaces. *Langmuir* **30**(14), 4033–4039 (2014). DOI 10.1021/la500312q. PMID: 24673164 [1](#)

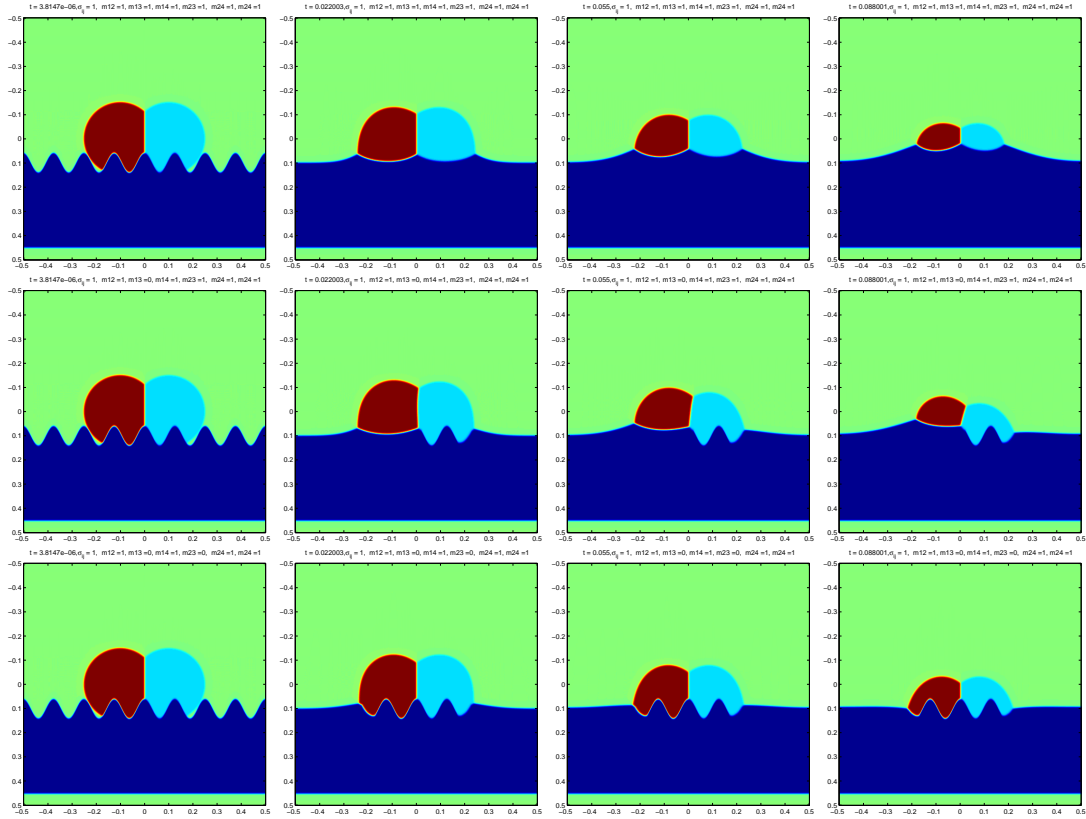


FIGURE 7. Numerical experiments with $N = 4$ phases. homogeneous surface tensions $\sigma_{ij} = 1$. The rows correspond to $(m_{12}, m_{13}, m_{14}, m_{23}, m_{24}, m_{34})$ equals to $(1, 1, 1, 1, 1, 1)$, $(0, 1, 1, 1, 1, 1)$ and $(0, 0, 1, 1, 1, 1)$ respectively. The graphs represent $u_1 + 3u_2 + 1.5u_4$ at different times, u_1, u_2, u_3 and u_4 are shown in light blue, red, blue and green, respectively.

- [8] Bence, J., Merriman, B., Osher, S.: Diffusion generated motion by mean curvature. Computational Crystal Growers Workshop, J. Taylor ed. Selected Lectures in Math., Amer. Math. Soc. pp. 73–83 (1992) 2
- [9] Bonnetier, E., Bretin, E., Chambolle, A.: Consistency result for a non monotone scheme for anisotropic mean curvature flow. Interfaces Free Bound. **14**(1), 1–35 (2012). DOI 10.4171/ifb/272. URL <https://doi.org/10.4171/ifb/272> 9
- [10] Bonnetier, E., Chambolle, A.: Computing the equilibrium configuration of epitaxially strained crystalline films. SIAM J. Appl. Math. **62**(4), 1093–1121 (2002). DOI 10.1137/S0036139900368571. URL <https://doi.org/10.1137/S0036139900368571> 1
- [11] Brassel, M., Bretin, E.: A modified phase field approximation for mean curvature flow with conservation of the volume. Mathematical Methods in the Applied Sciences **34**(10), 1157–1180 (2011). DOI 10.1002/mma.1426. URL <http://dx.doi.org/10.1002/mma.1426> 2
- [12] Bretin, E., Danescu, A., Penuelas, J., Masnou, S.: Multiphase mean curvature flows with high mobility contrasts: A phase-field approach, with applications to nanowires. Journal of Computational Physics **365**, 324 – 349 (2018). DOI <https://doi.org/10.1016/j.jcp.2018.02.051>. URL <http://www.sciencedirect.com/science/article/pii/S0021999118301426> 1, 4, 6, 9
- [13] Bretin, E., Denis, R., Lachaud, J.O., Oudet, E.: Phase-field modelling and computing for a large number of phases. ESAIM Math. Model. Numer. Anal. **53**(3), 805–832 (2019). DOI 10.1051/m2an/2018075. URL <https://doi.org/10.1051/m2an/2018075> 3, 6, 9
- [14] Bretin, E., Masnou, S.: A new phase field model for inhomogeneous minimal partitions, and applications to droplets dynamics. Interfaces and Free Boundaries (2017) 3
- [15] Caginalp, G., Fife, P.C.: Dynamics of layered interfaces arising from phase boundaries. SIAM J. Appl. Math. **48**(3), 506–518 (1988). DOI 10.1137/0148029. URL <http://dx.doi.org/10.1137/0148029> 6
- [16] Cahn, J.W.: Critical point wetting. The Journal of Chemical Physics **66**(8), 3667–3672 (1977). DOI <http://dx.doi.org/10.1063/1.434402>. URL <http://scitation.aip.org/content/aip/journal/jcp/66/8/10.1063/1.434402> 1

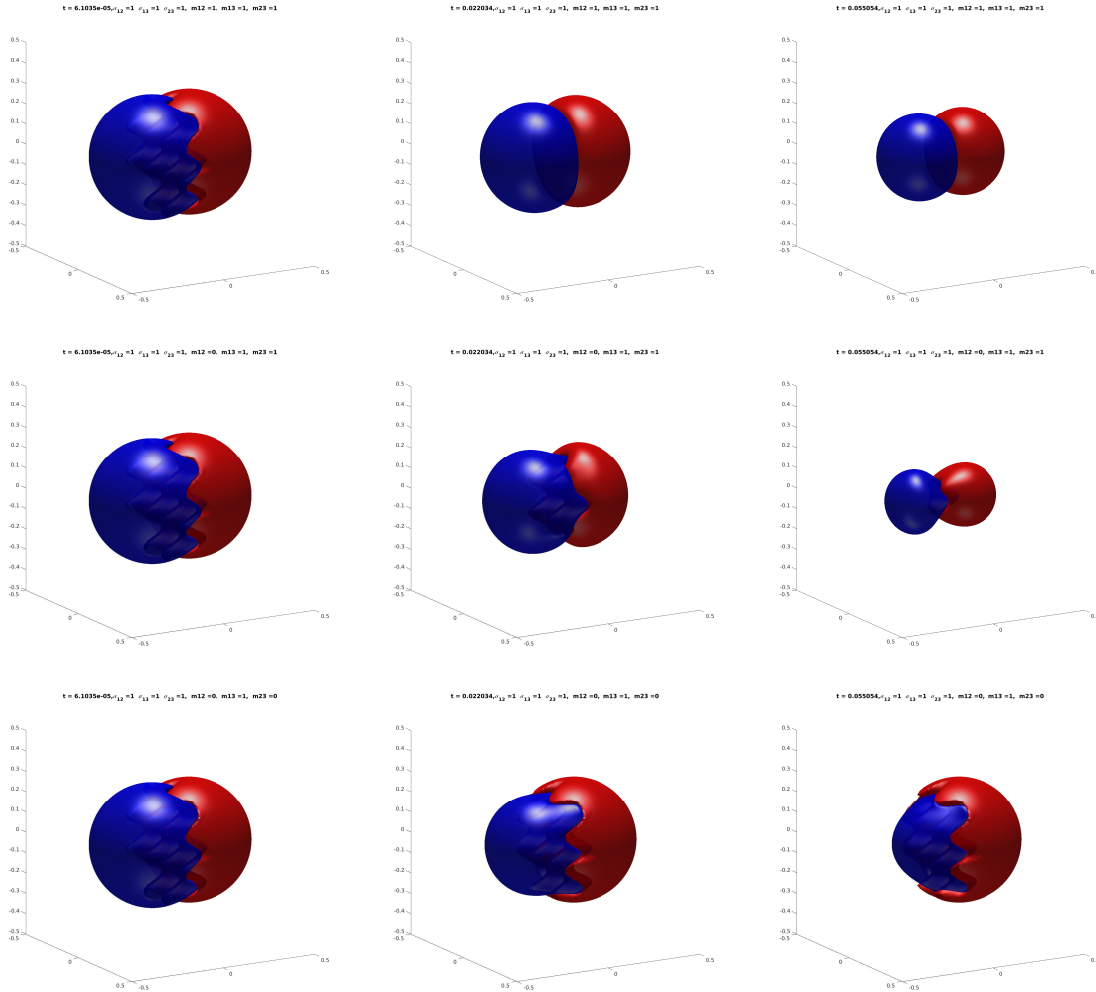


FIGURE 8. 3D experiments : In each case $\sigma_{12} = \sigma_{13} = \sigma_{23} = 1$; The rows correspond to $(m_{12}, m_{13}, m_{23}) = (1, 1, 1)$, $(m_{12}, m_{13}, m_{23}) = (0, 1, 1)$ and $(m_{12}, m_{13}, m_{23}) = (0, 1, 0)$ respectively. Each graph represents the level set $\{u_1 = 1/2\}$ in blue, and the level set $\{u_2 = 1/2\}$ in red, at different times.

- [17] Chen, L., Shen, J.: Applications of semi-implicit Fourier-spectral method to phase field equations. *Computer Physics Communications* **108**, 147–158 (1998) [8, 9](#)
- [18] Chen, X.: Generation and propagation of interfaces for reaction-diffusion equations. *J. Differential Equations* **96**(1), 116–141 (1992) [2](#)
- [19] Eyre, D.: *Computational and mathematical models of microstructural evolution*. Warrendale: The Material Research Society (1998) [9](#)
- [20] Garcke, H., Nestler, B., Stoth, B.: On anisotropic order parameter models for multi-phase systems and their sharp interface limits. *Physica D: Nonlinear Phenomena* **115**(1-2), 87 – 108 (1998). DOI [http://dx.doi.org/10.1016/S0167-2789\(97\)00227-3](http://dx.doi.org/10.1016/S0167-2789(97)00227-3). URL <http://www.sciencedirect.com/science/article/pii/S01672789970022733>
- [21] Garcke, H., Nestler, B., Stoth, B.: A multi phase field concept: Numerical simulations of moving phase boundaries and multiple junctions. *SIAM J. Appl. Math* **60**, 295–315 (1999) [3](#)
- [22] Garcke, H., Nestler, B., Stoth, B.: A multiphase field concept: numerical simulations of moving phase boundaries and multiple junctions. *SIAM J. Appl. Math.* **60**(1), 295–315 (2000). DOI [10.1137/S0036139998334895](https://doi.org/10.1137/S0036139998334895). URL <https://doi.org/10.1137/S00361399983348953>
- [23] Gilbarg, D., Trudinger, N.: *Elliptic Partial Differential Equations of Second Order*. Springer (1998) [6](#)
- [24] Loreti, P., March, R.: Propagation of fronts in a nonlinear fourth order equation. *European Journal of Applied Mathematics* **11**, 203–213 (2000). DOI null. URL http://journals.cambridge.org/article_S09567925990041316,7
- [25] Modica, L., Mortola, S.: Un esempio di Γ -convergenza. *Boll. Un. Mat. Ital. B* (5) **14**(1), 285–299 (1977) [1, 2](#)

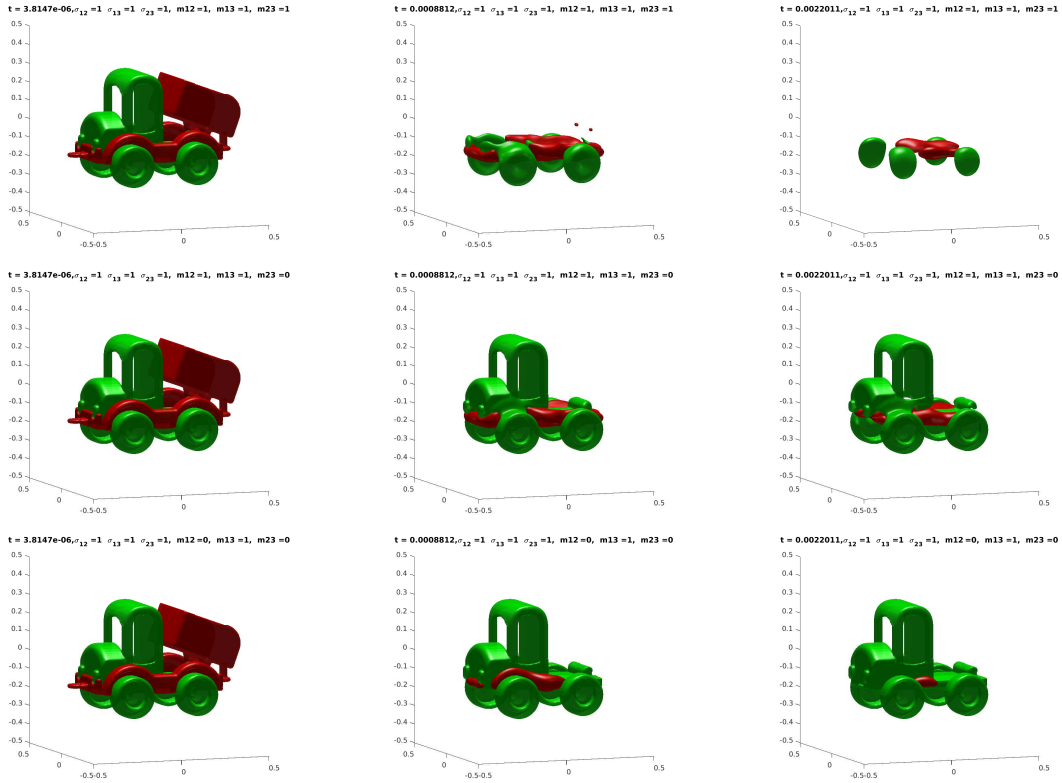


FIGURE 9. 3D experiments, identical surface tensions. The rows correspond to $(m_{12}, m_{13}, m_{23}) = (1, 1, 1)$, $(m_{12}, m_{13}, m_{23}) = (1, 1, 0)$ and $(m_{12}, m_{13}, m_{23}) = (0, 1, 0)$ respectively. The graphs depict the $1/2$ -level sets of u_1 (red) and u_2 (green).

- [26] de Mottoni, P., Schatzman, M.: Geometrical evolution of developed interfaces. *Trans. Amer. Math. Soc.* **347**, 1533–1589 (1995) [2](#)
- [27] Mullins, W.W.: *Two-Dimensional Motion of Idealized Grain Boundaries*, pp. 70–74. Springer Berlin Heidelberg, Berlin, Heidelberg (1999) [1](#)
- [28] Oudet, E.: Approximation of partitions of least perimeter by Gamma-convergence: around Kelvin’s conjecture. *Experimental Mathematics* **20**(3), 260–270 (2011). URL <http://projecteuclid.org/euclid.em/13179244193>
- [29] Pego, R.L.: Front migration in the nonlinear Cahn-Hilliard equation. *Proc. Roy. Soc. London Ser. A* **422**(1863), 261–278 (1989) [6](#)
- [30] Ruuth, S.J.: Efficient algorithms for diffusion-generated motion by mean curvature. *J. Comput. Phys.* **144**(2), 603–625 (1998). DOI [10.1006/jcph.1998.6025](https://doi.org/10.1006/jcph.1998.6025). URL <http://dx.doi.org/10.1006/jcph.1998.6025>
- [31] Shen, J., Wang, C., Wang, X., Wise, S.M.: Second-order convex splitting schemes for gradient flows with ehrlich-schwoebel type energy: Application to thin film epitaxy. *SIAM J. Numerical Analysis* **50**(1), 105–125 (2012) [9](#)
- [32] Takasao, K.: Convergence of landau-lifshitz equation to multi-phase brakke’s mean curvature flow. preprint [3](#)
- [33] Wang, N., Upmanyu, M., Karma, A.: Phase-field model of vapor-liquid-solid nanowire growth. *Phys. Rev. Materials* **2**, 033402 (2018). DOI [10.1103/PhysRevMaterials.2.033402](https://doi.org/10.1103/PhysRevMaterials.2.033402). URL <https://link.aps.org/doi/10.1103/PhysRevMaterials.2.033402>

INSTITUT FOURIER, UNIVERSITÉ GRENOBLE-ALPES, CS 40700, 38058 GRENOBLE CEDEX 09, FRANCE
Email address: eric.bonnetier@univ-grenoble-alpes.fr

UNIV LYON, INSA DE LYON, CNRS UMR 5208, INSTITUT CAMILLE JORDAN, 20 AVENUE ALBERT EINSTEIN, F-69621 VILLEURBANNE, FRANCE
Email address: elie.bretin@insa-lyon.fr

UNIV LYON, UNIVERSITÉ CLAUDE BERNARD LYON 1, CNRS UMR 5208, INSTITUT CAMILLE JORDAN, 43 BOULEVARD DU 11 NOVEMBRE 1918, F-69622 VILLEURBANNE, FRANCE
Email address: masnou@math.univ-lyon1.fr